Journal of Materials Chemistry B

Accepted Manuscript

ROYAL SOCIETY OF CHEMISTRY

www.rsc.org/materialsB

Chitosan-modified silver@ruthenium hybrid nanoparticles: evaluation of physico-chemical properties and bio-affinity with sialic acid

Murugan Veerapandian,[a] X. X. Zhu,[a,*] Suzanne Giasson[a,b,*]

Hybrid nanoparticles (NPs) integrated with dye molecules has attracted interest for biomolecular detection, due to their effortless fabrication, timely operation, controllable specific recognition and low-cost. In this study, hybrid core-shell NPs made of metal-dye complex (AgNPs@$[Ru(bpy)_3]^{2+}$) core and chitosan (CS) shell exhibiting selective fluorescence quenching effect were successfully prepared using a cost-effective wet-chemical approach. The physico-chemical properties of NPs were determined by spectroscopy and light scattering measurements. The bio-affinity of the AgNPs@$[Ru(bpy)_3]^{2+}$/CS was evaluated in aqueous media using sialic acid (SA) as target molecule in the presence of different monosaccharides and anionic biomolecules as interferents. A significant fluorescence quenching of hybrid NPs was observed in aqueous solutions of SA with interferents, while no significant quenching effect was detected in SA-free interferents solutions. The selective binding of SA to the particles resulted from favorable electrostatic interactions and inter-molecular hydrogen bonding with the functional groups of CS. The hybrid NPs system displayed a good sensitivity for SA with a detection limit of 5.1 nM and a concentration dependent fluorescence quenching for SA concentrations ranging from 25 nM to 3.2 μM. This hybrid NPs system represents a promising alternative probe for detecting sialic acid in complex samples.

1. Introduction

Development of novel hybrid nanoparticles (NPs) system is the topic of extensive research due to their synergistic physico-chemical and biological functionality suitable for diverse applications.[1,2] Specifically, the synthesis of hybrid AgNPs has received substantial attention because of their exploitable features such as high electrical, thermal conductivity, surface enhanced Raman scattering (SERS), chemical stability, catalytic activity, optical and redox behavior.[3] Besides, Ag composites exhibit broad-spectrum antibacterial and fungicidal activity, this makes them useful in biomedical industries.[4,5] Parallel to this area, composites of metallic dye complex such as tris(2,2'-bipyridyl)ruthenium (II) ($[Ru(bpy)_3]^{2+}$) constitutes a vast field of research with applications ranging from antitumor activity to electronic devices, fluorescence quenching, non linear optical properties and photocatalysis.[6-8] Owing to its large Stokes fluorescent shift, significant emission quantum yields, photochemical and thermal stability, and quenching property, nanocomposites of ruthenium (II) complexes are often utilized in analytical studies.[9]

Coating a thin layer of polymer on the surface of metal NPs is another area of potential interests to enhance the functional properties (biocompatibility, bio-affinity and biosensing) of nanosystem.[1,5,10] Among the several polymeric materials, chitosan (CS) has already demonstrated potential in the fabrication of a novel nanocomposite for biosensor.[11] CS is a bio-derived linear polysaccharide composed of randomly distributed β-(1-4)-2-amino-2-deoxy-D-glucopyranose (D-glucosamine) repeat unit. Three reactive groups, i.e., the primary amine group (C-2) and primary (C-6) and secondary (C-3) hydroxyl groups on each repeat unit of glucosamine residues allow CS to be modified for several bioapplications.[12,13] For instance, plasmonic efficiency of AgNPs and quantum dots coated with CS can be used for single-molecule detection and pathogen biosensing, respectively.[14,15]

Recent studies highlighted the ability to selectively organize the domains of metallic composite and polymeric materials into single "hybrid" nanosystem to modulate their physico-chemical and biological properties.[1,2,16] For instance, ruthenium (II) complex-modified Au, SiO_2-Ag and SiO_2NPs have shown important photophysical and thermo-sensitivity.[17-19] In parallel, CS-modified plasmonic NPs such as Ag and Au have exhibited interesting functionalities such as molecular sensing and anti-bacterial activity.[14,20,21] Further, CS modified NPs (SiO_2, Au/TiO_2, Au/MnO_2, Fe_3O_4 and TiO_2/CdS) and composites (AuNPs/nafion and carbon nanotubes/polymer) have shown much interest owing to their potential applications for electrochemical immunosensing.[22]

Inspired by the properties of aforementioned materials, herein we aimed to prepare a hybrid NPs system composed of AgNPs@$[Ru(bpy)_3]^{2+}$ modified with CS (AgNPs@$[Ru(bpy)_3]^{2+}$/CS) for potential bio-affinity studies. A simple but versatile wet-chemical approach was utilized to prepare the hybrid NPs, following a sequential reduction reaction, electrostatic and coordination chemistry. The prepared NPs system consist of metal (Ag) and dye complex ($[Ru(bpy)_3]^{2+}$) as the core and biopolymer (CS) as the shell. Understanding the physico-chemical properties is important to explore the new functionalities of the final material. The optical properties of AgNPs@$[Ru(bpy)_3]^{2+}$ such as absorbance and fluorescence emission upon surface modification with CS polymer are useful for such biosensing system. Morphology, chemical group, particle size distribution and zeta potential analysis were performed to elucidate the structural integrity of the nanosystem. From the experimental analysis, we observed that the CS modification not only provided new functional groups but also modified the inherent fluorescence properties of AgNPs@$[Ru(bpy)_3]^{2+}$ by exhibiting quenching.

This new structural functionality and quenching property was utilized further to explore the bio-affinity of AgNPs@$[Ru(bpy)_3]^{2+}$/CS with a model biomolecule sialic acid (SA). SA is an anionic monosaccharide also known as N-acetylated derivative of neuraminic acid. The normal range of total SA level in serum/plasma is 1.58-2.22 mmol L^{-1}, the free form of SA constituting 0.5-3 μmol L^{-1} and the lipid-associated SA is 10-50 μmol L^{-1}.[23] Due to its wide existence in biological fluids, tissues, and important role in expressing the functions of glycoconjugates, SA is recognized as the vital marker for several types of clinical symptoms including cancer,[24] cardiovascular disease[25] and diabetes.[26] Moreover, the bio-affinity of AgNPs@$[Ru(bpy)_3]^{2+}$/CS was also studied using common interferents such as glucose, galactose, ascorbic acid and gluconic acid δ-lactone. Intrinsic properties of the new hybrid NPs system such as fluorescence quenching behavior and bio-affinity toward the SA molecule are discussed based on the hybrid's surface-chemical functionality, charge affinity and large surface area.

2. Experimental Section

2.1 Materials

Silver nitrate ($AgNO_3$), sodium borohydride ($NaBH_4$), 3-mercaptopropionic acid (3-MPA), tris(2,2'-bipyridyl)dichlororuthenium(II) hexahydrate, chitosan (low molecular weight: 50 000-190 000 g mol^{-1}; degree of deacetylation: 75-85%), N-acetylneuraminic acid

(synthetic, ≥95%) and phosphate buffered saline (PBS) were purchased from Sigma-Aldrich. Milli-Q water (18.2 MΩ) was used for all experiments. All other chemicals were of analytical grade and used as received without any further purification.

2.2 Synthesis of AgNPs stabilized with 3-MPA

Colloidal AgNPs stabilized with 3-MPA were prepared following a reported procedure[27] with slight modification as follows. 5 mL of $AgNO_3$ (0.1 M), 25 mL of 14 N aq. NH_4OH and 5 mL of 3-MPA (50 mM) were dissolved in 15 mL of deionized (DI) water (solution A). Separately, 5 mL of $NaBH_4$ (0.02 M) and 2 mL of 14 N aq. NH_4OH were dissolved in 15 mL of DI water (solution B). The above solutions A and B were slowly injected dropwise into the 300 mL of DI water over 30 min at room temperature with a magnetic stirring of 600 rpm. After 30 min of reaction time, the resulting colloidal solution containing AgNPs stabilized 3-MPA mixture was separated by centrifugation (at 13,000 rpm for 60 min). The particles were then washed twice with DI water and stored in DI water for further experimentation.

2.3 Preparation of $[Ru(bpy)_3]^{2+}$-coated AgNPs and CS modification

5 mL of AgNPs stabilized with 3-MPA (1 mg/mL) and 5 mL of ethanolic solution of $Ru(bpy)_3Cl_2$ (0.8 mg/mL) was added to a vial. The suspension was then left overnight under mild stirring, protected from light. As-prepared particles were centrifuged (at 13,000 rpm for 60 min) and washed repeatedly with ethanol and DI water to remove the unreacted $[Ru(bpy)_3]^{2+}$. The $[Ru(bpy)_3]^{2+}$-coated AgNPs (AgNPs@$[Ru(bpy)_3]^{2+}$) were kept in aqueous dispersion for further surface modification and experimentation. CS solution was prepared by dissolving purified CS in 1% (w/v) acetic acid with aid of sonication. CS modification was achieved by allowing a simple coordination chemical reaction, between 5 mL of (1 mg/mL) AgNPs@$[Ru(bpy)_3]^{2+}$ and 5 mL of 0.01 wt% CS, under a magnetic stirring of 600 rpm for 3 hrs at room temperature. The final hybrid composed of AgNPs@$[Ru(bpy_3)]^{2+}$/CS were separated by centrifugation (at 13,000 rpm for 60 min), washed and redispersed in DI water with aid of sonication, and stored in DI water for characterization.

2.4 Quenching studies of AgNPs@$[Ru(bpy)_3]^{2+}$/ CS vs. SA

A stock solution of 1 mg/mL SA solution was prepared in PBS (pH 7.4) and stored in refrigerator. Solutions of appropriate concentration were prepared from this stock solution. For each quenching study, 1 mL of aqueous dispersion of AgNPs@$[Ru(bpy)_3]^{2+}$/CS (1 mg/mL), 1 mL of the desired SA solution and 1 mL of diluents were added to a vial and incubated at 4-8ºC for 3 hrs. After incubation, fluorescence emission spectra were recorded

from 500 to 800 nm upon excitation at 450 nm. All the experiments were replicated three times and the standard deviations were about 3%.

2.5 Characterization methods

UV-vis absorbance spectra were analyzed on a Cary 5000 UV-Vis-NIR spectrophotometer (Agilent Technologies). Morphological characterization was carried out with a transmission electron microscope (TEM) (Philips Tecnai 12) with an acceleration voltage of 120 kV. Samples used for the measurements were prepared by casting ~5 μL of (0.25 mg/mL) AgNPs or AgNPs@$[Ru(bpy)_3]^{2+}$ or AgNPs@$[Ru(bpy)_3]^{2+}$/CS suspension onto a carbon-coated nickel grid. Average particle size distribution of the prepared NPs and zeta potential of free NPs and NPs incubated with SA were studied with a Malvern dynamic light scattering (DLS)-Zetasizer Nano ZS instrument equipped with a 4 mW, 633 nm He-Ne laser, using appropriate cells. Measurements were conducted in backscattering (173º) mode and detected with an Avalanche photodiode. Thirteen runs were averaged for each liquid sample for accurate determination of size distribution and zeta-potential measurements. All the measurements were performed at 25ºC. Chemical structure and modification of functional groups were identified by Fourier transform-infrared (FT-IR) spectra recorded on a Nicolet 6700 FT-IR spectrometer (in the ATR mode, diamond crystal). Fluorescence emission spectra of aqueous solutions of $[Ru(bpy)_3]^{2+}$ dye, AgNPs@$[Ru(bpy)_3]^{2+}$ and AgNPs@$[Ru(bpy)_3]^{2+}$/CS were recorded with a Varian Cary Eclipse fluorescence spectrophotometer. Equilibrium dissociation constant (K_D) value for binding of selected monosaccharides to hybrid NPs were calculated by measuring the fluorescence emission intensity of hybrid NPs solution, in presence and absence of the analyte. Microplate reader Tecan Infinite M200® was used to measure the fluorescence emission intensity. All the samples were prepared in corning 96 flat bottom black well plates. Experimental conditions: fluorescence top reading mode, excitation and emission wavelength at 450 and 605 nm, respectively, excitation and emission bandwidth of 9 and 20 nm, respectively, number of flashes 25 and integration time of 25 μs.

3. Results and discussion

3.1 Synthesis of hybrid NPs

Scheme 1 illustrates the step-wise preparation route for obtaining the hybrid NP. At first, the synthesis of the aqueous AgNPs was achieved by *in situ* reduction reaction and stabilization with 3-MPA. Based on the well-known metal-sulfur chemistry, thiol groups of

3-MPA readily form a stable bond with the Ag surface atoms under mild conditions.[27] Subsequently, aqueous $[Ru(bpy_3)]^{2+}$ complex can be successfully attached by electrostatic interactions with the COO^{-} groups of AgNPs stabilized with 3-MPA. The dye-modified NPs

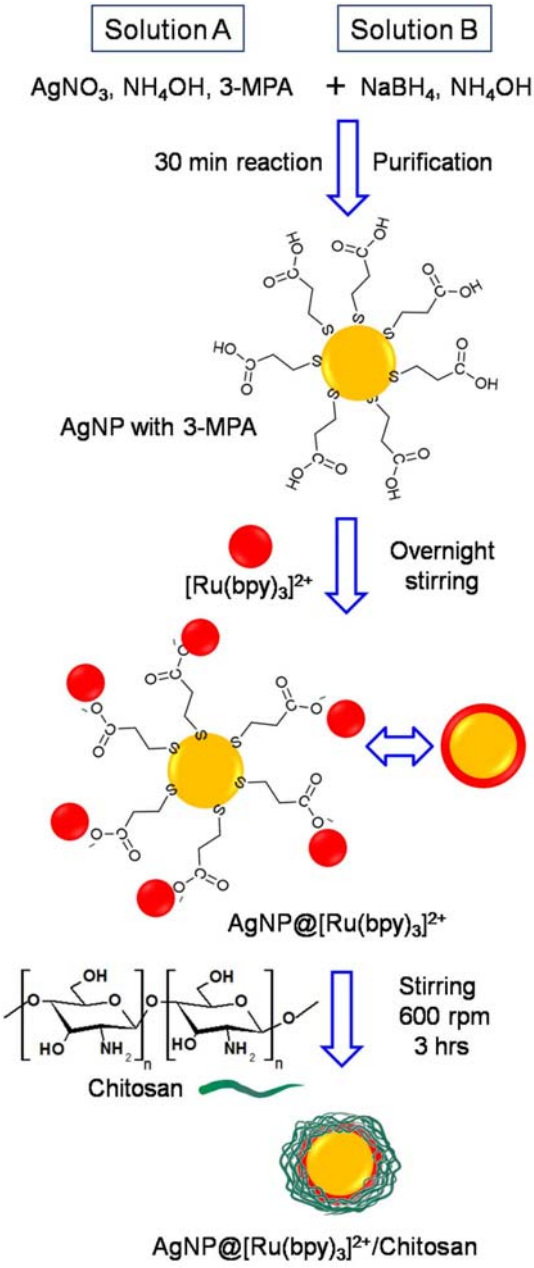

Scheme 1 Synthesis of AgNP stabilized with 3-MPA, dye $[Ru(bpy)_3]^{2+}$ complex coating on AgNP and chitosan modification on AgNP@$[Ru(bpy)_3]^{2+}$.

were then reacted with the CS solutions. Abundant amine groups of the CS molecule formed coordination bonds with the AgNPs@$[Ru(bpy)_3]^{2+}$ which in turn resulted in a final hybrid

structure (AgNPs@$[Ru(bpy)_3]^{2+}$/CS). The structural and chemical changes caused by the coordination reaction between AgNPs@$[Ru(bpy)_3]^{2+}$ and CS molecules were characterized by FT-IR spectroscopy as described later.

3.2. Characterization of particles

3.2.1 Morphological characterization

The TEM micrographs in Fig. 1 depict the representative images of NPs at three different stages of their preparation. The overall spherical shape of the final hybrid structure is maintained upon AgNPs reaction with $[Ru(bpy)_3]^{2+}$ and CS. At a higher magnification, the well-defined surface modification on NPs reveals the coating of CS molecules (Fig. 1G). The

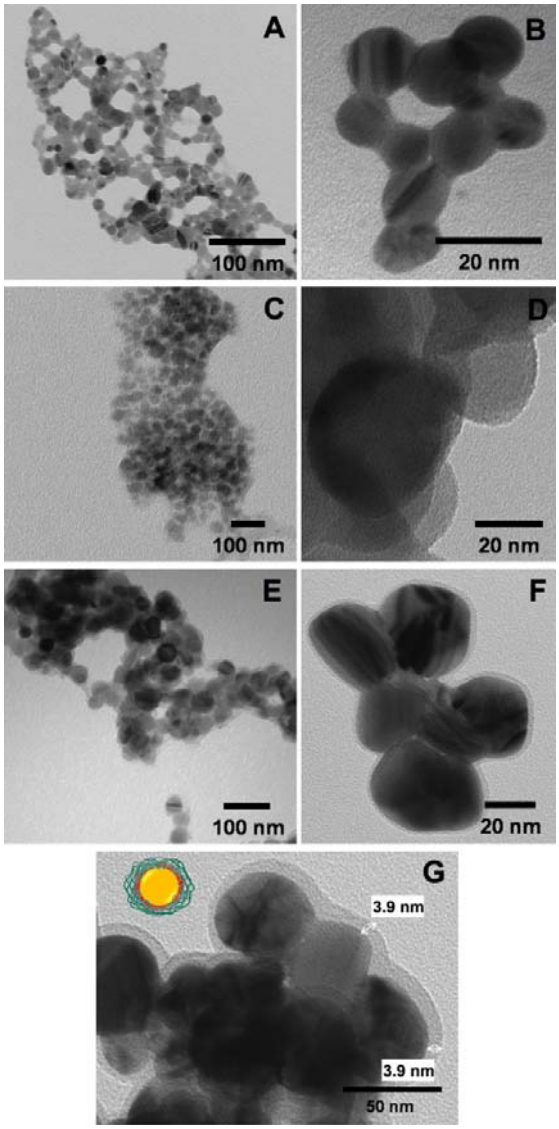

Fig. 1 TEM image of (A and B) AgNPs, (C and D) AgNPs@$[Ru(bpy)_3]^{2+}$ and (E, F and G) AgNPs@$[Ru(bpy)_3]^{2+}$/CS. The arrows in G indicate the thickness of CS layer. Inset drawing shows the expected morphology of AgNPs@$[Ru(bpy)_3]^{2+}$/CS.

thickness of CS layer on AgNPs@$[Ru(bpy)_3]^{2+}$ is ca. 3.9 nm. The particle size distribution was analyzed by DLS (Fig. 2). The average particle sizes of AgNPs, AgNPs@$[Ru(bpy)_3]^{2+}$ and AgNPs@$[Ru(bpy)_3]^{2+}$/CS are 13, 46 and 54 nm, respectively. These results are in good agreement with the size observed in TEM (Fig. 1).

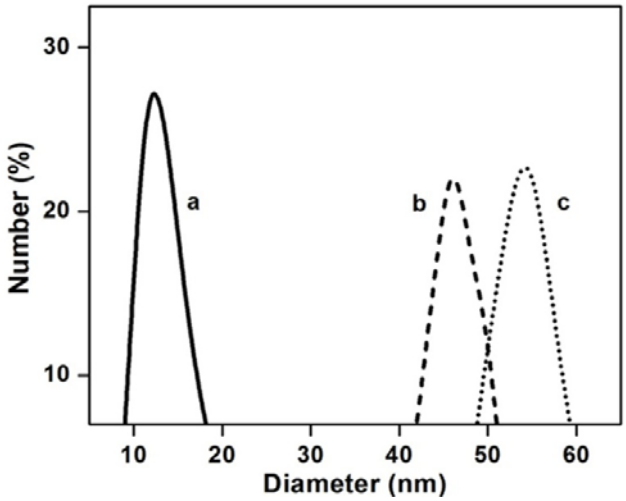

Fig. 2 A particle size distribution curve of (a) AgNPs, (b) AgNPs@$[Ru(bpy)_3]^{2+}$ and (c) AgNPs@$[Ru(bpy)_3]^{2+}$/CS determined by DLS measurement.

3.2.2 UV-vis absorbance and fluorescence

Fig. 3A shows the UV-vis absorption spectrum of aqueous dispersion of pristine AgNPs and AgNPs-MPA. The peak at 402 nm indicates the presence of characteristic surface plasmon resonance (SPR) of AgNPs. After surface modification with 3-MPA there is a significant red shift observed at 423 nm. It is known that factors such as particle size, shape, dielectric properties of the surrounding host matrix and solution can influence the oscillations of conductive electrons (responsible for SPR) present on the surface of metal NPs.[28] In the present case, introduction of 3-MPA altered the optical absorption of AgNPs. As shown in Fig. 3B, the UV-vis absorption spectrum of $[Ru(bpy)_3]^{2+}$ exhibits three specific peaks at 242, 290 and 450 nm attributed to intra-ligand transition $\pi \rightarrow \pi^*$, bpy $\pi \rightarrow \pi_1^*$ transition and metal-to-ligand charge-transfer (MLCT) band, respectively.[29] A shoulder peak at 420 nm is also ascribed to MLCT (t_{2g} (Ru)$\rightarrow\pi^*$ (bpy) transitions). Likewise, AgNPs modified with $[Ru(bpy)_3]^{2+}$ also exhibits three absorbance peaks with a moderate hump located at ~423 nm due to the overlap of SPR from AgNPs. This result agrees well with a previous study on $[Ru(bpy)_3]^{2+}$-coated Ag samples.[18] The NPs functionalized with CS exhibited a significant decrease in peak intensity. The peak centered at 450 nm is broadened, indicating the surface modification of the AgNPs@$[Ru(bpy)_3]^{2+}$ with CS. In the presence of SA, the hybrid NPs

system showed a further decrease in their absorbance due to the interaction of SA with the CS functional groups on the surface of hybrid NPs. The binding affinity between SA and AgNPs@$[Ru(bpy)_3]^{2+}$/CS will be addressed below in the section describing fluorescence quenching study.

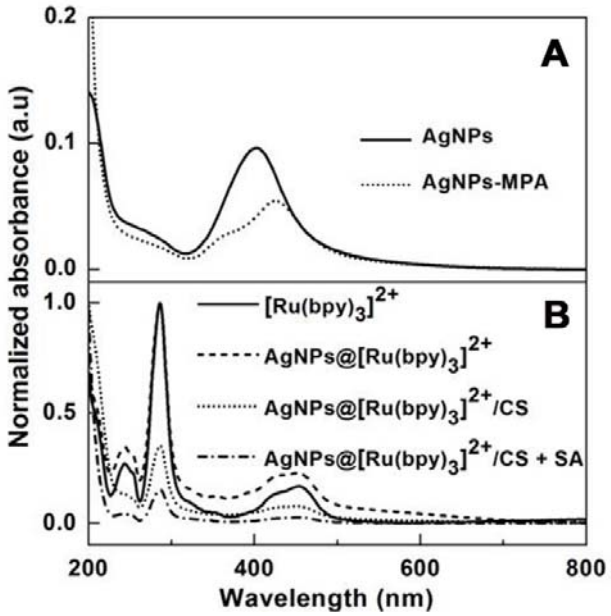

Fig. 3 UV-vis absorbance spectra of (A) AgNPs and AgNPs stabilized with 3-MPA. (B) Comparative spectra of aqueous $[Ru(bpy)_3]^{2+}$ dye, AgNPs@$[Ru(bpy)_3]^{2+}$, AgNPs@ $[Ru(bpy)_3]^{2+}$/CS and AgNPs@$[Ru(bpy)_3]^{2+}$/CS + SA solutions.

Fig. 4 compares the emission spectra of aqueous solutions of pristine $[Ru(bpy)_3]^{2+}$, AgNPs@$[Ru(bpy)_3]^{2+}$, AgNPs@$[Ru(bpy)_3]^{2+}$/CS and AgNPs@$[Ru(bpy)_3]^{2+}$/CS mixed with SA. The maximum fluorescence observed at 610 nm for $[Ru(bpy)_3]^{2+}$ is attributed to the emission from triplet MLCT excited state (^{3}MLCT) to the ground state.[29,30] AgNPs@$[Ru(bpy)_3]^{2+}$ showed a significant decrease in emission intensity with a slight shift (at 605 nm) compared to pristine dye molecules. This shift is associated with the interaction between the dye and the AgNPs surface. Dantham et al. discussed a similar static fluorescence quenching due to the charge transfer interaction between the AgNPs and other dyes like fluorescein 27 based on metal-OH ligand interaction.[31] The modification of CS led to a decreased emission intensity, indicating the occurrence of quenching. Mechanism associated with the peak shift and quenching effect can be related to the possible energy transfer between dye-coated metal NPs surface and amino groups of CS. Similar quenching behavior was observed earlier for other types of hybrid NPs such as fluorescent dye-modified

and CS-coated magnetic NPs.[32,33] The fluorescence is quenched further upon interaction with SA, denoting an affinity toward hybrid NPs system.

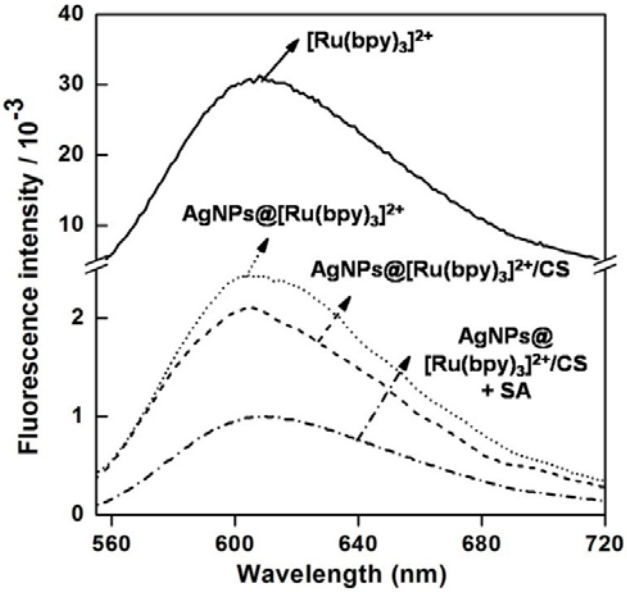

Fig. 4 Fluorescence emission spectra of $[Ru(bpy)_3]^{2+}$, AgNPs@$[Ru(bpy)_3]^{2+}$, AgNPs@ $[Ru(bpy)_3]^{2+}$/CS and AgNPs@$[Ru(bpy)_3]^{2+}$/CS + SA (λ_{ex}=450 nm) at room temperature.

3.2.3 FT-IR characterization

In order to investigate the attachment (physical adsorption or chemical bonding) between CS and AgNPs@$[Ru(bpy)_3]^{2+}$, a comparative FT-IR spectral study was performed. Inherent conformational stretching, bending vibrations of pristine CS and CS-modified AgNPs@$[Ru(bpy)_3]^{2+}$ were studied. Fig. 5A shows the FT-IR spectrum of pure CS powder with assigned functional groups such as C-H out of plane bend (887 cm^{-1}), C-O stretch (1026 and 1065 cm^{-1}), C-O-C stretch (1154 cm^{-1}), C-H bend (1377 cm^{-1}), N-H bend (1590 cm^{-1}), C-H stretch (2870 cm^{-1}), N-H stretch and hydrogen-bonded OH groups (3317 cm^{-1}), respectively.[34,35] Upon surface modification of AgNPs@$[Ru(bpy)_3]^{2+}$ with CS, the characteristic bands of CS exhibit significant alterations. For instance, notable changes in C-O stretch at 1040 cm^{-1} are observed in comparison with pristine CS. The peak attributed to primary N-H bend at 1590 cm^{-1} (Fig. 5A) is shifted to 1644 cm^{-1} (Fig. 5B), suggesting the formation of secondary amine. The new band at 2970 cm^{-1} is due to the asymmetric stretching of C-H group.[34] The peak for both N-H stretch and H-bonded OH stretch observed at 3311 cm^{-1} is much more intense than that observed for CS. Changes in the group frequencies (C-O stretch and N-H bend) of CS indicate their successful chemical bonding with AgNPs@$[Ru(bpy)_3]^{2+}$. This observation is supported by the previous studies on the

chemical reactivity between metal ions/metal NPs and active groups of CS such as primary OH (C-6), secondary OH (C-3) and amino groups (C-2).[12,36] Unlike physical adsorption, NPs system with chemically-attached polymer provides stability for durable biosensing applications.[37]

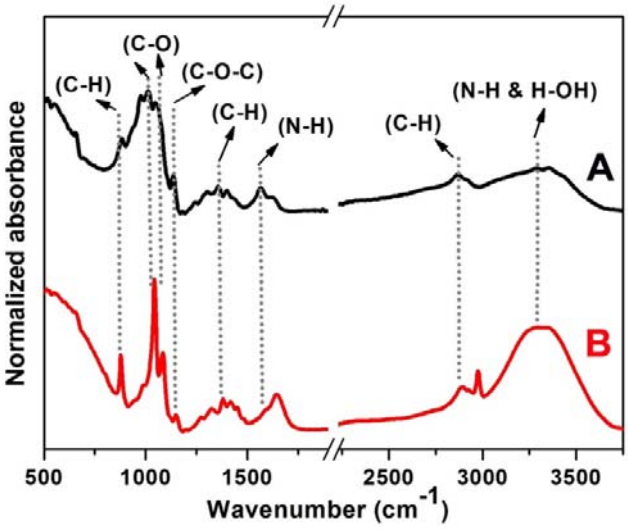

Fig. 5 ATR-FTIR spectra of (A) chitosan powder and (B) AgNPs@$[Ru(bpy)_3]^{2+}$/CS.

3.3 Fluorescence study

3.3.1 Fluorescence quenching with SA

SA binding to the NPs is expected to influence the fluorescence emission from the incorporated dye molecules as fluorescence quenching has shown to depend on the amount of binding moieties.[38] Fluorescence quenching of AgNPs@$[Ru(bpy)_3]^{2+}$/CS as a function of SA concentration is illustrated in Fig. 6A. The fluorescence intensity gradually decreases with increasing concentration of SA in the range from 0.025 to 3.5 μM. The equation for the calibration plot is $y = -0.511x+1079$ (where x is the concentration of sialic acid and y the fluorescence emission intensity) with a correlation coefficient of 0.957. According to the standard deviation 0.87 for the blank sample with 20 parallel measurements, a detection limit of 5.1 nM is calculated based on the three-times standard deviation rule.[39] The specific binding affinity of SA on the surface of CS-coated AgNPs@$[Ru(bpy)_3]^{2+}$ can be associated with electrostatic interaction and hydrogen bonding. As mentioned previously, SA is a negatively charged monosaccharide. On the other hand, abundant amine groups of CS on the surface of AgNPs@$[Ru(bpy)_3]^{2+}$ provide an overall positive surface potential to the final hybrid NPs, with a zeta potential of +45.1 mV (Supplementary Fig. S2). Therefore, SA could bind to the CS on the surface of hybrid NPs *via* electrostatic interactions. Furthermore, the

five hydroxyl groups of SA located at C-2, C-4, C-7, C-8 and C-9 positions can mediate hydrogen bonding with the reactive groups of CS.

To gain a deeper understanding of the binding affinity between AgNPs@$[Ru(bpy)_3]^{2+}$/CS and SA, the variation in zeta potential of AgNPs@$[Ru(bpy)_3]^{2+}$/CS as function of SA concentration was studied (Fig. 6B). Upon interaction with the negatively-charged SA, the zeta potential of the AgNPs@$[Ru(bpy)_3]^{2+}$/CS decreased from 45.1 mV in SA-free media (Fig.S2) to 19.4 mV for a SA concentration of 3.2 μM. Measurements with lower SA concentrations gave rise to higher values of zeta potential increasing steadily from 20.3 mV at 1.6 μM SA to 24.5 mV at 0.025 μM SA (see Fig. 6B). The change in surface potential observed from the binding of SA onto the surface of AgNPs@$[Ru(bpy)_3]^{2+}$/CS provides an additional evidence of the binding affinity of the analyte molecules and its concentration dependence.

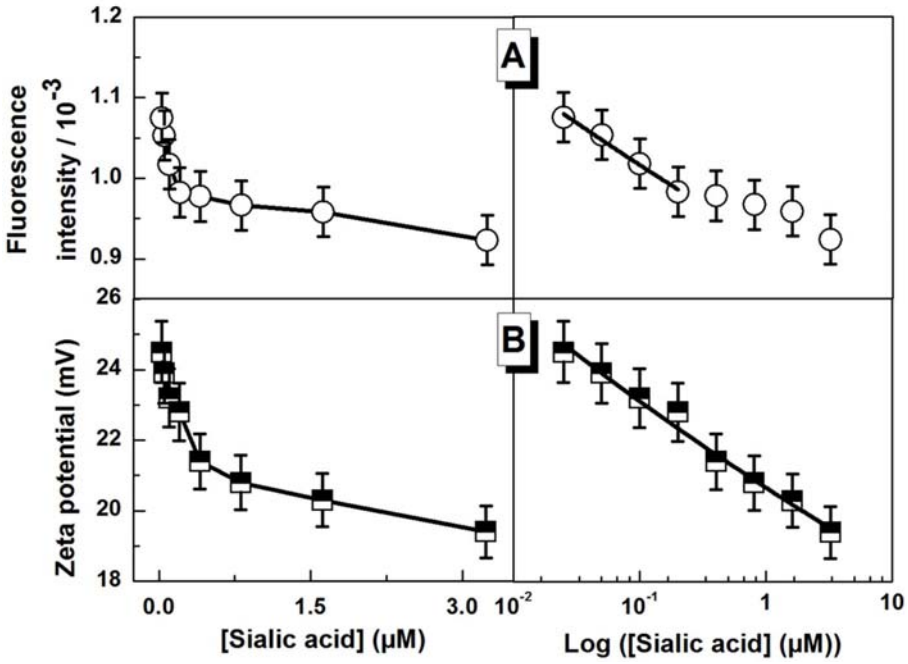

Fig. 6 (A) Fluorescence quenching effect of AgNPs@$[Ru(bpy)_3]^{2+}$/CS against different concentrations of incubated SA (from 0.025 to 3.2 μM). Measured fluorescence emission wavelength at 605 nm (λ_{ex} at 450 nm), at room temperature. (B) Zeta potential of AgNPs@$[Ru(bpy)_3]^{2+}$/CS in presence of different concentrations of SA from 0.025 to 3.2 μM. Each data point represents the average of three independent measurements, and error bars represent the standard deviation of the mean.

3.3.2 Effect of interferents

We have also studied the fluorescence quenching behavior of AgNPs@$[Ru(bpy)_3]^{2+}$/CS in the presence of other monosaccharide molecules such as glucose and galactose. Three different concentrations of interferent molecules were prepared with PBS buffer as diluents (pH 7.4) and incubated with hybrid NPs. Fig. S5A shows the plots of fluorescence emission intensity of the hybrid NPs incubated with interferents. The quenching effect of hybrid NPs incubated with different concentrations of glucose and galactose is insignificant, while mixed interferents including SA mediated a significant quenching effect from hybrid NPs. The weak interaction between glucose/galactose and the surface of hybrid NPs is explained by equilibrium dissociation constant (K_D) described in the following section. The specificity of AgNPs@$[Ru(bpy)_3]^{2+}$/CS for SA detection was further examined by the introduction of two negatively-charged compounds, L-ascorbic acid and D-(+)-gluconic acid δ-lactone. Ascorbic acid is known as an important interferent compound in human body fluids. On the other hand D-(+)-gluconic acid δ-lactone is a neutral compound, but hydrolyzes in water to gluconic acid which is acidic in nature. The resulting fluorescence intensity induced by L-ascorbic acid, D-(+)-gluconic acid δ-lactone and SA (each at a concentration of 1 g/L) is shown in Fig. S5B. It is clear that SA induced the most significant fluorescence quenching (ca. 50%), indicating a stronger interaction with the particles due to cooperative effects of multiple functional groups of SA.

3.3.3 Determination of K_D

The fluorescence quenching method has been successfully used to determine the non-covalent binding affinities between ligands (i.e., chlorogenic, ferulic and gallic acids, quercetin, rutin, and isoquercetin) and receptors (i.e., human serum albumin, bovine serum albumin, soy glycinin, and lysozyme).[40] In this study, a similar method was used to determine the binding affinity between selected biomolecules (SA, L-ascorbic acid, D-(+)-gluconic acid δ-lactone, D-(+)-glucose and D-(+)-galactose) and the hybrid NPs. The K_D value was determined using the one-site total binding model[40,41] with the following equation:

$$\Delta F = \frac{(F_0 - F_\infty)L_0}{K_D + L_0}$$

where F_0 and F are the fluorescence emission intensity of the hybrid NPs solution, in the absence and presence of the analyte, respectively, $\Delta F = F_0 - F$, F_∞ is the NPs fluorescence intensity saturated with the ligand, and L_0 the total concentration of the bound and unbound ligand (analyte).[40,41] The decrease in NPs fluorescence in the presence of different

concentrations of the analyte is measured and the dissociation constant as well as the value for maximum fluorescence difference ($\Delta F_{max}=F_0-F_\infty$) are calculated from the above equation. The data were fitted using GraphPad Prism software version 5.0 (GraphPad Software, Inc.) and the K_D values were calculated using nonlinear regression analysis (Fig. 7A-B). Fig. 7A shows that, with SA at approximately 250 µM, the ΔF value for hybrid NPs reaches a plateau. The K_D values obtained from the model with one-site total binding assay for SA, L-ascorbic acid, D-(+)-gluconic acid δ-lactone, D-(+)-glucose and D-(+)-galactose are 24.4 ± 7.1, >70, >236, >551 and >764 µM, respectively. As the K_D is inversely proportional to K_A (equilibrium association constant) a lower K_D value denotes a better binding affinity between

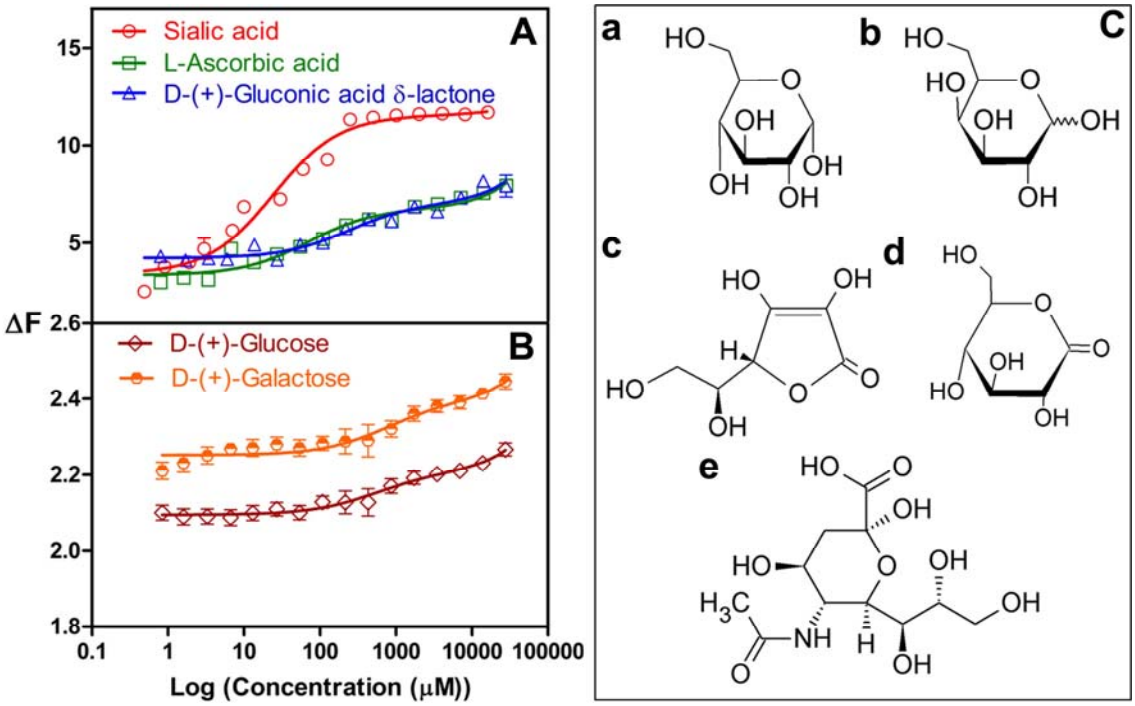

Fig. 7 (A-B) Determination of K_D using the quenching of the AgNPs@$[Ru(bpy)_3]^{2+}$/CS fluorescence. Concentration of sialic acid, L-ascorbic acid, D-(+)-gluconic acid δ-lactone, D-(+)-glucose and D-(+)-galactose ranges from 500 to 0.014 µg/mL; CS-modified AgNPs@$[Ru(bpy)_3]^{2+}$ at a concentration of ~0.46 µg/mL. Fluorescence emission intensity measured at the wavelength of 605 nm (λ_{ex} 450 nm) at room temperature. Each data point represents the average of three independent measurements and error bars represent the standard deviation of the mean. Where error bars are not visible, they are comparable to the size of the symbols. **(C)** The chemical structures of (a) D-(+)-glucose, (b) D-(+)-galactose, (c) L-ascorbic acid, (d) D-gluconic acid δ-lactone and (e) N-acetylneuraminic acid (SA).

the receptor and ligand. The lowest K_D value of SA indicates the highest binding affinity between SA and hybrid NPs system. All the compounds studied possess hydroxyl groups in common, which might contribute in binding with CS layer on the surface of hybrid NPs through hydrogen bonding. However, in addition to the hydroxyl groups, SA contains a carboxylic acid and a secondary amine group. Due to its multiple functional groups, SA providing a better binding affinity toward the hybrid NPs.

3.3.4 pH effect

CS is a pH-sensitive biopolymer with a p*Ka* of ~6.5.[42] Protonated and deprotonated–NH_2 groups are favored at low (<6.5) and high (>6.5) pH respectively.[43] Spectral properties of fluorescent molecules are known to be pH dependant.[44] Therefore, fluorescence quenching of the hybrid NPs is expected to depend on pH. Fluorescence measurements on AgNPs@$[Ru(bpy)_3]^{2+}$/CS aqueous dispersion were carried out at several pH and SA concentrations (Fig. S6A). The fluorescence emission intensities of the hybrid NPs and SA-incubated hybrid NPs did not significantly change in the pH range from 4.3 to 10.8. However, the hybrid NPs exhibited a SA concentration-dependent quenching behavior. Fluorescence measurements were also carried out in the presence of interferents to assess the SA specificity of hybrid NPs at different pH values. The degree of fluorescence quenching observed from the hybrid NPs incubated with SA and interferents is larger than that of the samples incubated only with interferents (Fig. S6B). Moreover, the quenching behavior of hybrid NPs incubated with SA (1 μg/mL) and with mixtures of interferents (glucose, galactose and SA, each at 1 μg/mL) are similar (Fig. S6). These results suggest that the developed system has good specificity towards the SA in a concentration-dependent manner regardless of pH.

4. Conclusion

The new hybrid core-shell NPs show selective binding with nanomolar affinity for SA. The results showed that the CS shell of AgNPs@$[Ru(bpy)_3]^{2+}$ could selectively bind the SA molecules in the presence of selected common interferents in a concentration-dependent manner regardless of the pH. The highest binding affinity between SA and hybrid NPs system was confirmed from the equilibrium dissociation constant. The three-in-one (metal, dye complex and biopolymer) NPs system enabled a lowest detection limit of 5.1 nM SA. The hybrid NPs system demonstrated advantages for its ease in synthesis and operation, low

cost, reproducibility and bio-affinity toward SA. For improvement of hybrid NPs sensitivity as well as stability, the adsorption properties of dye $[Ru(bpy)_3]^{2+}$ and CS, including the density derived fluorescence quenching, need to be further studied.

Acknowledgments

Financial support from NSERC of Canada and FQRNT of Quebec is acknowledged. M. Veerapandian thanks the GRSTB for postdoctoral scholarship. The authors are members of GRSTB funded by FRSQ.

Notes and references

[a]Department of Chemistry, [b]Faculty of Pharmacy, Université de Montréal
CP 6128, Succursale Centre-ville, Montreal, QC, H3C 3J7, Canada
E-mail: julian.zhu@umontreal.ca (X.X. Zhu), suzanne.giasson@umontreal.ca (S. Giasson)

† Electronic Supplementary Information (ESI) available: [TEM image and SAED pattern of AgNPs, zeta potential and AFM image of AgNPs@$[Ru(bpy)_3]^{2+}$/CS, ATR-FT-IR of AgNPs@$[Ru(bpy)_3]^{2+}$, fluorescence quenching of hybrid NPs: effect of interferents and pH].

1. K. Santhosh Kumar, V.B. Kumar and P. Paik, *Journal of Nanoparticles*, 2013, Article ID 672069.
2. C. Sanchez, C. Boissiere, S. Cassaignon, C. Chaneac, O. Durupthy, M. Faustini, D. Grosso, C. Laberty-Robert, L. Nicole, D. Portehault, F. Ribot, L. Rozes and C. Sassoye, *Chem. Mater.,* 2014, **26**, 221.
3. Q.H. Tran, V.Q. Nguyen and A.-T. Le, *Nanotechnology,* 2013, **4**, 033001.
4. M. Ahamed, M.S. Alsalhi and M.K. Siddiqui, *Clin. Chim. Acta,* 2010, **411**, 1841.
5. W. Xiao, J. Xu, X. Liu, Q. Hu and J. Huang, *J. Mater. Chem. B,* 2013, **1**, 3477.
6. K. E. Erkkika, D. T. Odom and J. K. Barton, *Chem. Rev.,* 1999, **99**, 2777.
7. T. Le Bouder, O. Maury, A. Bondon, K. Costuas, E. Amouyal, I. Zyss and H. Le Bozec, *J. Am. Chem. Soc.,* 2003, **125**, 12284.
8. C.R. Mayer, E. Dumas and F. Se´cheresse, *Chem. Commun.,* 2005, 345.
9. L. Tormo, N. Bustamante, G. Colmenarejo and G. Orellana, *Anal. Chem.,* 2010, **82***,* 5195.
10. H.S. Mansur, A.A. P. Mansur, E. Curtib and M.V. De Almeida, *J. Mater. Chem. B*, 2013, **1**, 1696.
11. S.K. Shukla, A.K. Mishra, O.A. Arotiba and B.B. Mamba, *Int. J. Biol. Macromol.,* 2013, **59**, 46.

12. M.E.I. Badawy and E.I. Rabea, *Int. J. Carbohydr. Chem.,* 2011, Article ID 460381.
13. G.B. Jung, J.-H. Kim, J.S. Burm and H.K. Park, *Appl. Surf. Sci.*, 2013, **273**, 179.
14. M. Potara, M. Baia, C. Farcau and S. Astilean, *Nanotechnology,* 2012, **23**, 055501.
15. H.N. Abdelhamid and H.F. Wu, *J. Mater. Chem. B,* 2013, **1**, 6094.
16. M.N. Tahir, F. Natalio, M.A. Cambaz, M. Panthofer, R. Branscheid, U. Kolb and W. Tremel, *Nanoscale,* 2013, **5**, 9944.
17. M. Jebb, P. K. Sudeep, P. Pramod, K. George Thomas and P.V. Kamat, *J. Phys. Chem. B,* 2007, **111**, 6839.
18. K. Mori, M. Kawashima, M. Cheand H. Yamashita, *Angew. Chem. Int. Ed.,* 2010, **49**, 8598.
19. M. Mirenda, V. Levi, M.L. Bossi, L. Bruno, A.V. Bordoni, A.E. Regazzoni and A. Wolosiuk, *J. Colloid Interf. Sci.,* 2013, **392**, 96.
20. M. Potara, D. Maniu and S. Astilean, *Nanotechnology*, 2009, **20**, 315602.
21. M. Potara, E. Jakab, A. Damert, O. Popescu,V. Canpean and S. Astilean, *Nanotechnology,* 2011, **22**, 135101.
22. W. Suginta, P. Khunkaewla and A. Schulte, *Chem. Rev.*, 2013, **113**, 5458.
23. P. Sillanaukee, M. Ponnio and I. P. Jaaskelainen, *Eur. J. Clin. Invest.,* 1999, **29**, 413.
24. K. Matsuno and S. Suzuki, *Anal. Biochem.,* 2008, **375**, 53.
25. K.P. Gopaul and M.A. Crook, *Clin. Biochem.,* 2006, **39**, 667.
26. G.S. Vahalkar and V.A. Haldankar, *Int. J. Clin. Biochem.,* 2008, **23**, 223.
27. K. Mori, A. Kumami, M. Tomonari and H. Yamashita, *J. Phys. Chem. Lett*., 2009, **113***,* 16850.
28. M. Veerapandian, S.K. Lim, H.M. Nam, G. Kuppannan and K.S. Yun, *Anal. Bioanal. Chem.,* 2010, **393**, 867.
29. P. Innocenzi, H. Kozuka and T. Yoko, *J. Phys. Chem. B,* 1997, **101***,* 2285.
30. A. Juris, V. Balzani, F. Barigelletti, S. Campagna, P. Belser and A. Von Zelewsky, *Coord. Chem. Rev.,* 1988, **84**, 85.
31. V.R. Dantham, P.B. Bisht, B.S. Kalanoor, T.T. Baby and S. Ramaprabhu, *Chem. Phys. Lett.,* 2012, **521**, 130.
32. L. Li, D. Chen, Y. Zhang, Z. Deng, X. Ren, X. Meng, F. Tang, J. Ren and L. Zhang, *Nanotechnology*, 2007, **18**, 405102.
33. Y. Ge, Y. Zhang, S. He, F. Nie, G. Teng and N. Gu, *Nanoscale Res. Lett.,*2009, **4**, 287.

34. J. Coates, Interpretation of infrared spectra, a practical approach, in: Meyers, R.A., (Ed.), Encyclopedia of Analytical Chemistry. John Wiley and Sons Ltd., Chichester, UK, 2000, 10815.
35. J.D. Liao, S.-P. Lin and Y.T. Wu, *Biomacromolecules,* 2005, **6**, 392.
36. H. Jiang, Z. Chen, H. Cao and Y. Huang, *Analyst,* 2012, **137**, 5560.
37. P. Kannan and S. Abraham John, *Biosens. Bioelectron.,* 2011, **30**, 276.
38. S. Jiwpanich, B.S. Sandanaraj and S. Thayumanavan, *Chem. Commun.,* 2009, **7**, 806.
39. D.W. Huang, C.-G. Niu, G.-M. Zeng and M. Ruan, *Biosens. Bioelectron.,* 2011, **29**, 178.
40. H.M. Rawel, S.K. Frey, K. Meidtner, J. Kroll and F.J. Schweigert, *Mol. Nutr. Food Res.,* 2006, **50**, 705.
41. D.E. Epps, T.J. Raub, V. Caiolfa, A. Chiari and M. Zamai, *J. Pharm. Pharmacol.*, 1999, **51**, 41.
42. K.M. Varum, M.H. Ottoy and O. Smidsrod, *Carbohydr. Polym.,* 1994, **25**, 65.
43. D.W. Lee, H. Lim, H.N. Chong and W.S. Shim, *The Open Biomaterials Journal* 2009, **1**, 10.
44. J. H. Lee, J. Je, J. Hur, M.A. Schlautman and E.R. Carraway, *Analyst*, 2003,**128**, 1257.

Table of contents entry

Hybrid nanoparticle system composed of silver, ruthenium and chitosan for selective recognition of sialic acid based on fluorescence quenching